Molecular Dynamics Simulation of Size-Dependent Structural and Thermal Properties of Polymer Nanofibers

Sezen Curgul,[†] Krystyn J. Van Vliet,[†] and Gregory C. Rutledge*,[‡]

Department of Materials Science and Engineering, Massachusetts Institute of Technology, Cambridge, Massachusetts 02139, and Department of Chemical Engineering, Massachusetts Institute of Technology, Cambridge, Massachusetts 02139

Received July 2, 2007; Revised Manuscript Received August 30, 2007

ABSTRACT: We present the results of molecular dynamics (MD) simulations of amorphous polymer nanofibers to study their size-dependent properties. The fibers consist of chains that mimic the prototypical polymer polyethylene, with chain lengths ranging between 50 and 300 carbons (C50 to C300). These nanofibers have diameters in the range 1.9 to 23.0 nm. We analyzed these nanofibers for signatures of emergent behavior in their structural and thermal properties as a function of diameter. The mass density at the center of all fibers is constant and comparable to that of the bulk polymer. The surface layer thickness ranges from 0.78 to 1.39 nm for all fibers and increases slightly with fiber size. The calculated interfacial excess energy is 0.022 ± 0.002 J/m^2 for all of the nanofibers simulated. The chains at the surface are more confined compared to the chains at the center of the nanofiber; the latter acquire unperturbed dimensions in sufficiently large nanofibers. Consistent with experiments and simulations of amorphous polymer films of nanoscale thickness, the glass transition temperature of these amorphous nanofibers decreases with decreasing fiber diameter, and is independent of molecular weight over the range considered.

Introduction

Electrospinning of polymeric nanofibers is a promising approach for development and commercialization of one-dimensional (1-D) nanomaterials. The small fiber diameter (50−500 nm) and large surface area (10−100 m^2/g) of such polymeric nanofibers offer a new class of materials that can be used in diverse applications including filters, composites, fuel cells, catalyst supports, drug delivery devices, and tissue scaffolds. Of fundamental necessity for many of these applications is an understanding of the size dependence of properties in individual nanofibers. Indeed, one operational definition of a "nanofiber" is that it exhibits new, emergent behavior as the diameter of the fiber is decreased from macroscopic to microscopic length scales, typically in the nanometer range.

Individual polymeric nanofibers are challenging to characterize experimentally due to their small size. This is due in large part to the requirement that a single nanofiber be isolated and manipulated without introducing defects prior to physical or mechanical analysis. Atomistic computer simulations can be helpful in determining and predicting the properties of individual nanofibers, especially as a function of length scales that are comparable to molecular dimensions.

Various simulation techniques have been applied to investigate the confinement of polymeric systems in one or two dimensions. First, lattice Monte Carlo (MC) simulations of a melt−vacuum interface were performed by Madden using a film adsorbed on a solid surface.[1] The film was shown to have a central region with bulklike characteristics, sandwiched between two interfacial regions. The structural features at the interface were found not to scale with molecular weight. Using off-lattice atomistic simulation, Mansfield et al. identified regions of thickness 1.0 nm at the surfaces of a thin film of atactic polypropylene of thickness 6.1 nm, in which local structural features were different from the bulk.[2] Again, no dependence of structural properties on the molecular weight (MW) was found in the interfacial region, for the MW range 1068−3246 g/mol. Short time scale dynamics of the atactic polypropylene−vacuum interface were then studied using molecular dynamics (MD) simulations.[3] While the structural features were in agreement with molecular mechanics results,[2] enhancements in the mean-squared displacement of the atoms relative to the chain center of mass were observed in the near-surface region, compared to the bulk polymer. Harris[4] observed chain end segregation and flattening of chains at the liquid-vacuum interface in MD simulations of thin films comprising short-chain alkanes, and off-lattice MC simulations of thin films showed that chains exhibit predominantly bulklike characteristics at the film center and are more collapsed at the vacuum surface.[5] MD simulations of thin films of poly(1,4-*cis*-butadiene) showed that the sharp onset of orientation of the backbone bonds corresponds with the drop in mass density from its bulk value.[6] A thicker surface layer was found in MD simulations of amorphous polyethylene (PE) than in thin films of poly(1,4-*cis*-butadiene), which was attributed to the stiffer nature of the PE chains.[7] A dynamic MC simulation method on a high coordination lattice was subsequently introduced by Mattice and co-workers[8] and used to determine equilibrium and dynamic properties of amorphous PE thin films.[9,10] It was observed that the segregation of chain ends contributed to increased mobility at the free surface of PE thin films.[11] The decrease in radius of gyration of chains was more significant for free-standing PE thin films as the molecular weight increased.[12]

While there have been numerous studies of nanometer-thick films by simulation, to our knowledge, only two studies of polymer nanofibers have been reported to date.[13,14]Both of these employed the coarse-grained MC method on a high coordination lattice that was used previously for thin films[8−10] and nanoparticles.[15] Two PE nanofibers with diameters 5.6 and 7.6 nm were

* Corresponding author. E-mail: rutledge@mit.edu.
[†] Department of Materials Science and Engineering, Massachusetts Institute of Technology.
[‡] Department of Chemical Engineering, Massachusetts Institute of Technology.

10.1021/ma0714666 CCC: $37.00
Published on Web 10/20/2007

simulated[13] on a high coordination lattice, with interactions between occupied lattice sites designed to account for both short and long range interactions. It was found that the density profiles of these nanofibers could be fitted to a hyperbolic tangent profile, and there was significant segregation of end beads to the surface. Molecules were found to orient preferentially parallel to the surface, with the largest principal axis parallel to the surface. Diffusion coefficients of 5.6×10^{-6} nm^2/Monte Carlo step in the narrower nanofiber and 4.4×10^{-6} nm^2/Monte Carlo step for the thicker nanofiber were calculated for 1-D diffusion parallel to the fiber axis.[14] The mobility of the chains at the surface of the PE nanofiber was found to be greater than that of the chains at the center of the nanofiber. The overall chain mobility was found to increase as the fiber size decreased. Similar trends were observed for the free-standing thin films,[10] implying that the curvature present in the fibers does not have a significant effect on the diffusion characteristics of the chain segments. The increased mobility in both the nanofibers and in the free-standing thin films was attributed to a region of lower mass density at the surface.

All of the above studies suggest that when polymers are confined in one or two dimensions, structural properties and dynamics show significant changes compared to those in bulk. These differences have implications for the properties of such materials confined on the nanometer length scale. For example, the glass transition temperature (T_g) of amorphous polymer thin films has been observed either to increase or decrease with decreasing film thickness,[16−28] phenomena that have attracted great interest in recent years as part of a larger effort to understand the nature of the glass transition itself. The first systematic study of the dependence of the T_g on film thickness in thin polymer films was performed by Keddie et al. using ellipsometry.[16] A series of polystyrene (PS) films of thicknesses between 10 and 200 nm were prepared on silicon wafers and reductions in T_g for films with thicknesses less than 40 nm were measured. Results obtained for PS films on a variety of substrates using numerous experimental techniques such as ellipsometry,[16,17] dielectric spectroscopy,[18,19] X-ray reflectivity,[20] local thermal analysis[21] and probe fluorescence intensity measurements[22,23] show a consistent decrease in T_g with decreasing film thickness. However, a modest increase in T_g was observed with decreasing film thickness for PMMA films on silicon oxide, demonstrating the importance of polymer−substrate interactions on the measured T_g.[24] This interfacial control of physical properties is also demonstrated by the greater decrease in T_g observed for free-standing thin films, compared to films adhered to some substrates.[25−28]

Numerous simulation studies have been conducted to reveal the underlying mechanism of the glass transition in spatially confined polymers. Torres et al. have demonstrated in MD simulations that the diffusivity of polymer segments is highly heterogeneous in polymer thin films, and that it is strongly correlated with deviations of T_g from the bulk.[29] An unentangled polymer melt confined between two repulsive walls was studied using MD simulations, and the reduction in T_g upon decreasing film thickness was explained by the faster chain dynamics due to the presence of the smooth walls.[30−32] Yoshimoto et al.[33] employed nonequilibrium MD simulations using a coarse grained polymer model to show that mechanically soft layers are formed near the free surfaces of glassy thin films and that T_g also decreased as the film thickness decreased.

In the present work, the effects of confinement and curvature on the structural and thermal properties of polyethylene nanofibers are investigated. Our aim is to evaluate these properties as a function of fiber diameter. In this way, we expect to develop a fundamental understanding of the extent and origin of fiber properties that emerge with decreasing diameter.

Simulation Details

Model. We performed MD simulations of prototypical PE fibers using a large-scale atomic /molecular massively parallel simulator (LAMMPS), a classical molecular dynamics code designed to run efficiently on parallel computers.[34] LAMMPS is flexible in the sense that it can be used with several different force fields and interaction parameters. We use the united atom model of Paul et al.[35] for PE, in which the hydrogen atoms are combined with the carbon atoms to which they are attached. This force field has been shown to give an accurate description of PE melts, as well as reasonable crystallization and melting transitions for *n*-alkanes.[35−37] The force field potential can be represented as follows:

$$\Phi = k_b(l - l_0)^2 + k_a(\theta - \theta_0)^2 + \sum_{i=1}^{3} \frac{1}{2} k_i[1 - \cos i\phi] + 4\epsilon\left[\left(\frac{\sigma}{r}\right)^{12} - \left(\frac{\sigma}{r}\right)^{6}\right] \quad (1)$$

In the equation above, the first term is the harmonic bond stretching potential where $k_b = 1.464 \times 10^5$ kJ/mol nm^2 and $l_0 = 0.153$ nm is the equilibrium C−C bond length. The second term is the harmonic bond angle bending potential, where $k_a = 251.04$ J/mol deg^2 is the angle bending parameter and $\theta_0 = 109.5°$ is the equilibrium C−C−C bond angle. The third term is the bond torsion potential, which accounts for all intramolecular interactions between atoms separated by three bonds. The parameters for this term are as follows: $k_1 = 6.77$ kJ/mol; $k_2 = -3.627$ kJ/mol; $k_3 = 13.556$ kJ/mol. The last term is the Lennard-Jones (LJ) potential, which is used to compute the nonbonded interactions between all united atom pairs that are on different chains or that are separated by four or more bonds on the same chain. The nonbonded potential parameters are as follows: $\epsilon(CH_2-CH_2) = 0.391$ kJ/mol; $\epsilon(CH_3-CH_3) = 0.948$ kJ/mol; $\epsilon(CH_2-CH_3) = 0.606$ kJ/mol; $\sigma = 0.401$ nm (for all united atom types). The cutoff distance for all nonbonded interactions was achieved with a smooth spline fit of the LJ potential to zero at $r = 1$ nm.

In our simulations, the prototypical chainlike molecule consists of 50−300 carbon atoms (C50−C300). The simulation box length in the fiber axis direction, L_z, was chosen just short enough to suppress the growth of Rayleigh instabilities on the time scale of the simulation, typically $L_z < 2\pi R_{fiber}$, where R_{fiber} is the expected fiber radius. The initial bulk density for all systems was 0.75 g/cm^3 at 495 K. A time step of 1 fs was used. The simulations were run for durations of 5−25 ns to characterize the relaxation times for different polymer chain lengths and to obtain equilibrated structures at the end of each stage of simulation (bulk and fiber). The total size of the systems varied between 200 and 150 000 carbons.

Simulation Procedure. The nanofiber was constructed by the following method. First a simulation of desired size N (number of united atom groups) and cubic volume ($V = L_xL_yL_z$) was created, with periodic boundary conditions employed in all three Cartesian directions, such that the density was 0.75 g/cm^3. This system, which corresponds to the "bulk state", was simulated using LAMMPS. After equilibration in the bulk state, the box dimensions L_x and L_y were increased simultaneously by a factor of 3−4, such that the molecules no longer interacted with their images in these expanded directions. The system then interacts with its images only in one dimension; under these

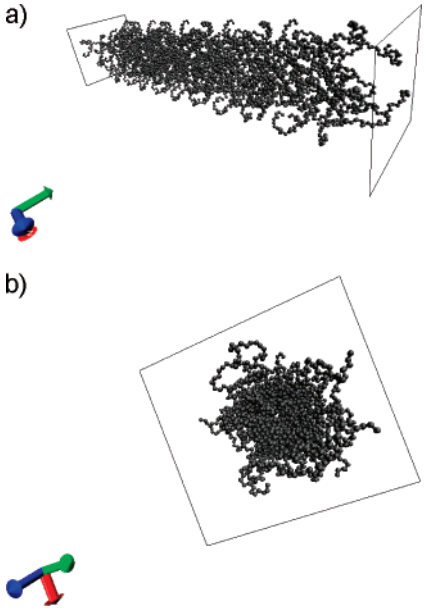

Figure 1. 20×C50 polyethylene nanofiber at 495 K. The representative volume element includes 20 chains, each comprising 50 carbon atoms. (a) Inclined to fiber longitudinal axis. Five periodic images in the axial direction are included for clarity. (b) Fiber cross-section. The fiber diameter is 3.54 nm. Planar areas are drawn as guides to the eye.

conditions, a cylindrically symmetric free surface spontaneously formed upon further equilibration, resulting in a section of a nanofiber. If the nanofiber is considered to be a cylinder, the *z*-direction along which the simulation box is still periodic becomes the "fiber axis" or the "axial" direction of the fiber. The other two orthogonal directions, *x* and *y*, or any linear combination of these, become "radial" directions, which were confirmed to be indistinguishable during simulation. Figure 1 shows two perspectives of a typical nanofiber generated in this way. Note that the fiber nomenclature reflects the number and length of chains within this representative volume element, or box: 20×C50 indicates 20 chains, each comprising 50 carbon atoms.

For the investigation of static properties, every system was simulated in an *NVT* ensemble at 495 K, which is well above the melting temperature of PE. For the investigation of the glass transition temperature of the fiber, the bulk structure was first cooled to 100 K in the *NPT* ensemble, with an effective cooling rate of 1.97×10^{10} K/s, and $P = 10^5$ N/m^2 and the configurations at a series of temperatures were saved. A previous simulation study[39] has shown that comparable cooling rates provide an estimate of the glass transition temperature that is ~30 K higher than the accepted experimental value; however, this offset should not significantly affect any trends in T_g. These configurations were then used as the initial configurations of the nanofiber at each temperature and the nanofibers were re-equilibrated in the *NVT* ensemble at each temperature. Only the axial dimension of the fiber is affected by the choice of ensemble; in all cases, the fiber radius is free to expand or contract, regardless of box size.

Comparison of the glass transition temperatures of the nanofiber and the thin film also required construction of thin film simulations. These thin films were constructed from the equilibrated "bulk" simulations by the same method used to create the fiber, but increasing the box dimension in only one direction instead of two.

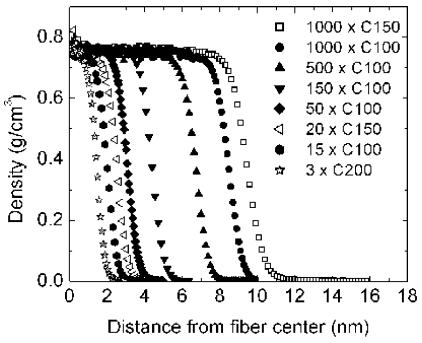

Figure 2. Density profiles extending from the fiber center provide a means to determine effective fiber diameter via the Gibbs dividing surface method. Here, fiber diameter can be varied via the number or molecular weight of the individual PE chains. $N \times Cm$ refers to N chains of length m united atoms.

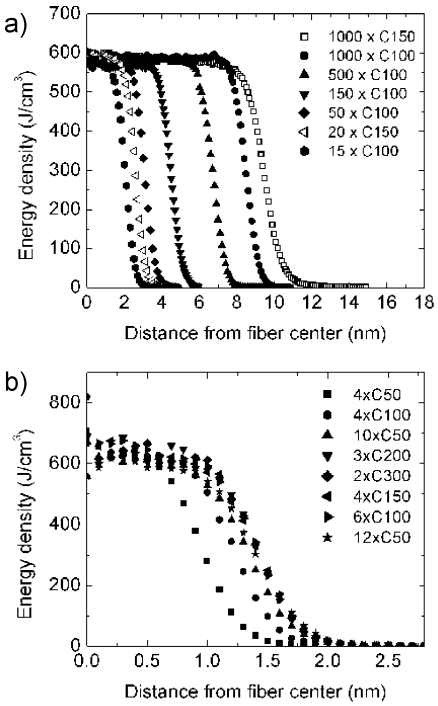

Figure 3. Energy density profiles extending from the fiber center to the surface enables the calculation of interfacial excess energy as a function of fiber size and molecular weight: (a) fibers with $R_{fiber} > 2.0$ nm. (b) Fibers with $R_{fiber} < 2.0$ nm.

Results

Density Profile. For our simulations, the density profile is important in defining the surface and core regions of the fiber. For this analysis, the fiber was divided into cylindrically symmetric bins (shells) of 0.1 nm width, starting from the center of the fiber. The number of atoms that fall into each shell was counted and normalized by the shell volume. This procedure was carried out for each snapshot and the ensemble averaged number density profile was calculated. This value was then converted to mass density of the fiber. The results for several systems are shown in Figure 2. As Figure 2 shows, the density within the core of the fiber spontaneously assumes the bulk density of the polymer. The increased fluctuation in density near $r = 0$ is a consequence of poorer statistical sampling for bins of small radius, but does not affect any of our conclusions. The mass density profiles for systems with the same total number of carbons are nearly identical, indicating that this result is insensitive to molecular weight.

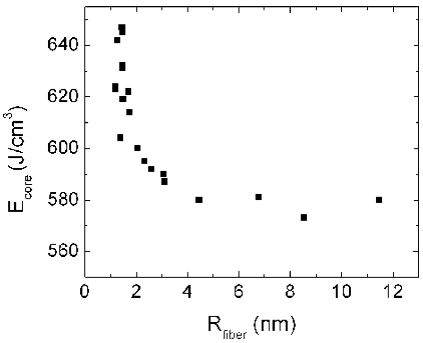

Figure 4. Energy at the fiber core E_{core} depends on fiber radius. This is illustrated for a simulation temperature of 495 K.

Table 1. Diameter and Interfacial Thickness Values for Simulated PE Nanofibers at 495 K

system	L_z (nm)	diameter (nm)	interfacial thickness (nm)
3×C200	2.6	2.908	1.03
15×C100	3.6	4.112	1.06
20×C150	4.5	5.218	1.15
50×C100	5.4	6.2	1.21
150×C100	7.9	8.9	1.13
500×C100	11.4	13.528	1.25
1000×C100	14.6	17.054	1.32
1000×C150	16.7	22.95	1.39

The fiber diameter was determined using the Gibbs dividing surface method (GDS). We adopted the common definition of the Gibbs dividing surface wherein the integral of the mass density profile equals the integral of the step function that takes the values of core mass density or vacuum on either side of the GDS; this amounts to the conservation of mass. Hence, the interface mass density

$$2\pi \int_0^\infty (\rho(r) - \rho^{\text{step}}(r|r_{GDS}))r\, dr = 0 \tag{2}$$

vanishes for this particular definition of the dividing surface, whose location is $r_{GDS} = R_{fiber}$. For the fibers simulated in this work, the diameters $2r_{GDS}$ obtained by this method range from 1.88 to 22.95 nm. The reported value represents an average over the entire course of the simulation; analyses of temporal variations in diameter did not reveal any low-frequency fluctuations ("breathing modes"). The "90−10 interfacial thickness", *t*, which can be defined as the distance over which the mass density of the fiber decreases from 90% to 10% of the corresponding bulk value, is between 0.78 and 1.39 nm for all fibers studied at 495 K, and increases slightly with increasing fiber diameter. Table 1 summarizes these properties for various systems.

Interfacial Energy. The interfacial excess energy of the fibers can affect wetting characteristics and inter-fiber interactions. The enthalpic contribution to this quantity can be determined from the potential energy density, which is calculated by considering all interactions (bond stretching, angle bending, torsion, Lennard-Jones) and apportioning the energy for each interaction equally among the particles involved. Figure 3 shows the energy density profiles for several systems. In order to define interfacial energy, the true energy profile is replaced by a step function, where the step is located at the position r_{GDS} determined previously from the mass density profile. In general, the energy and mass density profiles do not coincide, and there is an excess energy at the interface that can be calculated as follows:

$$E_{int} = [E_{total} - E_{fiber}]/[2\pi r_{GDS} L] \tag{3}$$

where E_{int} is the interfacial excess energy and E_{fiber} is the energy of the fiber in the macroscopic limit, as defined below. *L* is an arbitrary length of the fiber. E_{fiber} and E_{total} are calculated from the following formulas:

$$E_{total} = 2\pi L \int_0^\infty E(r) r\, dr \tag{4}$$

$$E_{fiber} = E_{core} \pi r_{GDS}{}^2 L \tag{5}$$

where E_{core} is the energy density spontaneously adopted at the center or core of the fiber. E_{core} obtains a value of 580 J/cm^3 for fibers with $R_{fiber} > 2.0$ nm, equal to the bulk energy density determined from bulk simulations. For fibers with $R_{fiber} < 2.0$ nm, E_{core} increases by 10% (580−640 J/cm^3) as the fiber radius decreases. The increase of E_{core} is mainly due to the loss of attractive LJ interactions in fibers with $R_{fiber} < 2.0$ nm. Figure 4 shows E_{core} as a function of fiber radius.

The excess interfacial energy at 495 K was calculated to be $\sim 0.022 \pm 0.002$ J/m^2 and does not depend on the fiber radius. This value is similar to 0.02 J/m^2 (at 400 K) previously estimated by Mattice and co-workers for a thin film of PE, using their 2NND lattice model[7] and to 0.0254 J/m^2 (at 473 K) reported from experiments.[38] Experiments confirm a weak dependence of interfacial energy on temperature (-5.7×10^{-5} J/m^2/K) up to 1000 K,[38] indicating an extrapolated interfacial energy of 0.0241 J/m^2 at 495 K. Note that these simulated values are internal energies, rather than free energies.

Molecular Conformations. Our results from density and interfacial energy calculations show that surface properties can differ significantly from the properties at the center of the fiber. This may be attributed to perturbed conformations that the molecules take at the surface, under the influence of curvature and/or confinement. For this reason, we calculated the global equilibrium radius of gyration (R_g) values of chains within the fibers.

Figure 5 shows radius of gyration values normalized by bulk radius of gyration ($R_g/R_{g,bulk}$) for each molecular weight as a function of fiber radius, also normalized by the corresponding bulk radius of gyration ($R_{fiber}/R_{g,bulk}$). $R_{g,bulk}$ is calculated from the conformations of chains equilibrated in the melt phase. Normalized in this way, the primary effect of chain length is removed. The deviation of $R_g/R_{g,bulk}$ from unity as $R_{fiber}/R_{g,bulk}$ decreases is a signature of the effects of confinement on chain conformation. The confinement of chains is clearly indicated: for smaller nanofibers, there is significant deviation of $R_g/R_{g,bulk}$ from unity, which is more pronounced for longer chains. As the fiber size increases, the chains eventually acquire their $R_{g,bulk}$ values. It appears that chains confined within fibers having diameter less than 2 (for C50) to 4 (for C100) times the bulk radius of gyration are noticeably perturbed from their bulk state.

We also calculated the R_g of the chains as a function of the distance from the fiber center (Figure 6). These results suggest that the confinement of the chains penetrates from the free surface, over a distance $\sim R_g$ from the GDS toward the fiber center.

Glass Transition Temperature of Nanofibers. To determine the T_g of nanofibers, we employed a method that is commonly used in both experiments and simulations. We monitored the specific volume, which is related closely to the fiber radius, as a function of temperature. Since the liquid and the glassy states have different thermal expansion coefficients, specific volume(*T*) changes slope upon crossing T_g. We determine T_g as the

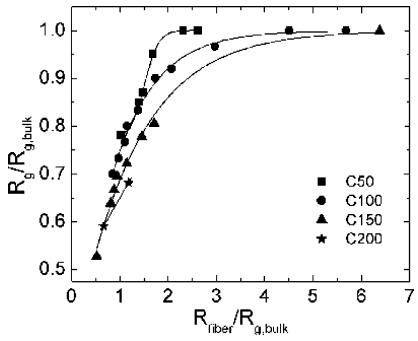

Figure 5. Normalized radius of gyration as a function of normalized fiber radius (at 495 K) shows significant confinement of the chains with increasing molecular weight and decreasing fiber size. Solid lines are intended to guide the eye.

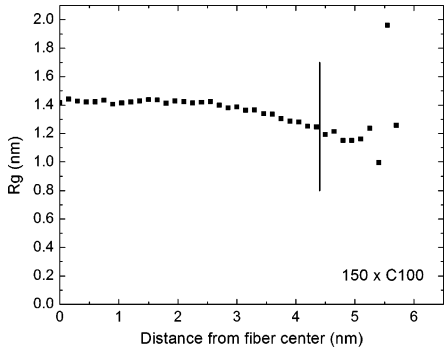

Figure 6. R_g vs distance from the fiber center shows that the confinement of chains penetrates over a distance approximately one R_g from the Gibbs dividing surface (GDS) to the fiber center. The vertical line represents the location of GDS.

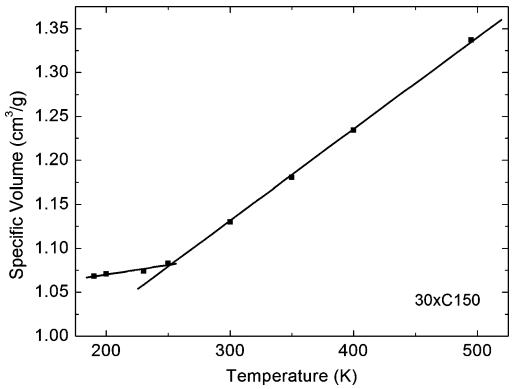

Figure 7. R_{fiber} vs temperature indicates T_g of 250 K for this nanofiber (R_{fiber} = 2.807 nm at 250 K).

intersection point of linear extrapolations from the liquid and glass sides; an illustration of this procedure is shown in Figure 7. Figure 8a shows the T_g as a function of the radius and thickness of fibers and free-standing thin films, respectively. For purposes of comparison, the fiber results are shown as a function of fiber radius R_{fiber} while the film results are shown as a function of film half-thickness ($h_{1/2}$).

As shown clearly in Figure 8a, the T_g of both the nanofibers and the free-standing films are depressed with decreasing radius or thickness. The thickness-dependent depression in T_g has been demonstrated experimentally and computationally[16,28] for a range of amorphous polymer thin films. Here, we observe similar behavior for amorphous polymer nanofibers.

To provide a physical interpretation for the depression of T_g in these nanofibers, we invoke a layer model similar to that

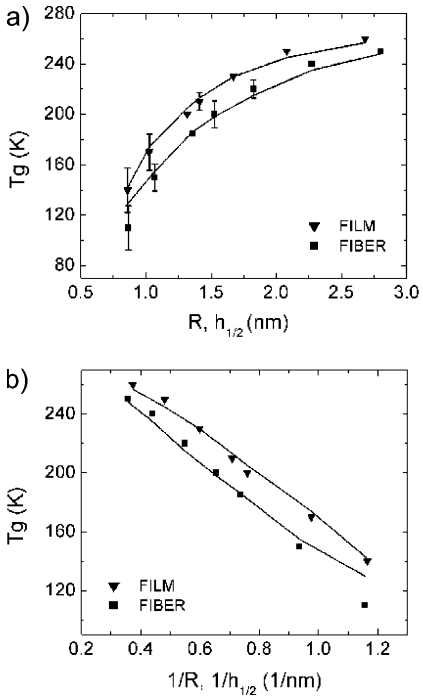

Figure 8. (a) T_g as a function of R_{fiber} (at $T = T_g$) for nanofiber and of $h_{1/2}$ (at $T = T_g$) for free-standing PE thin films shows the depression of T_g with decreasing fiber radius or film half-thickness. Solid lines are least-squares regression to data. (b) T_g as a function of $1/R_{fiber}$ for nanofiber and of $1/h_{1/2}$ for free-standing PE thin films. Solid lines show the best fit to the layer model discussed in the text.

proposed by Forrest and Mattson for low molecular weight free-standing thin films.[27] The model can be applied to other geometries such as cylinder, sphere and ellipsoid. (See Appendix.) This volume-averaged T_g formulation assumes a region near the free surface with enhanced mobility and depressed T_g ($T_{g,surf} < T_{g,bulk}$). For simplicity, $T_{g,surf}$ is assumed to be constant throughout the surface layer, although mobility may in fact vary within this layer. The thickness of this surface region is thought to be the same as the temperature-dependent length scale of cooperative motion for the glass transition dynamics, $\xi(T)$. Assuming a single T_g equal to the bulk value for the fiber core, the average T_g value of the free-standing thin film is written as follows:[27]

$$T_g = T_{g,bulk} - \frac{\xi(T_g)}{h_{1/2}}(T_{g,bulk} - T_{g,surf}) \quad (6)$$

The comparable expression for the nanofiber can be expressed as

$$T_g = T_{g,bulk} - \left[\frac{2\xi(T_g)}{R} - \left(\frac{\xi(T_g)}{R}\right)^2\right](T_{g,bulk} - T_{g,surf}) \quad (7)$$

Note that the factor of 2 in the linear term arises due to the 2-dimensional nature of confinement in the case of the nanofibers. (See Appendix.) A relation that accounts for the increase in the cooperativity length scale $\xi(T)$ with decreasing temperature is given by

$$\xi(T) = \xi(T_{ref}) + \sigma(T_{ref} - T)^{\gamma} \quad (8)$$

where σ and γ are empirical constants. A natural choice for T_{ref} was shown to be $T_{g,bulk}$, since the data can only be used to describe $\xi(T)$ for $T < T_{g,bulk}$.[27] We use the value $T_{g,bulk}$ = 280

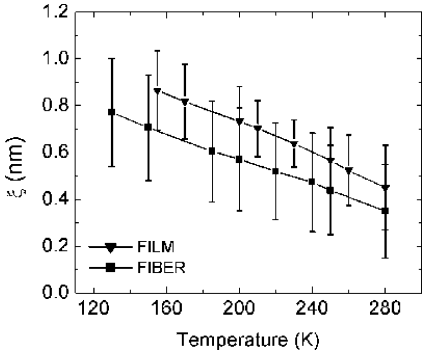

Figure 9. Cooperativity length scale $\xi(T)$ as a function of temperature for the nanofibers and free-standing PE thin films.

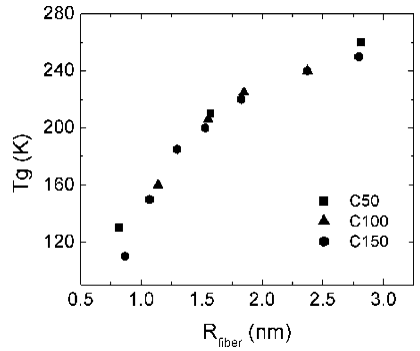

Figure 10. T_g as a function of R_{fiber} for molecular weights ranging from 700 (C50) to 2100 g/mol (C150) shows no significant dependence of T_g depression on molecular weight.

K, reported previously for the simulated bulk amorphous polyethylene (C768) using the same force field.[39]

Using eqs 6 and 7 to obtain a least-squares best fit to our results in Figure 8, we calculate $T_{g,surf} = 150 \pm 7$ K, $\xi(T_{g,bulk}) = 0.35 \pm 0.2$ nm, $\sigma = 0.4 \pm 0.1$ and $\gamma = 0.5 \pm 0.2$ for the nanofibers. Similarly, $T_{g,surf} = 155 \pm 5$ K, $\xi(T_{g,bulk}) = 0.45 \pm 0.18$ nm, $\sigma = 0.15 \pm 0.02$ and $\gamma = 0.7 \pm 0.0$ for the thin films. The solid lines in Figure 8, parts a and b, represent the best fit T_g data using these constants. Figure 9 shows $\xi(T)$ calculated from these parameters, indicating a statistically insignificant difference between this cooperativity length scale in the nanofibers and thin films. The layer theory thus predicts a single cooperativity length for both geometries, which is $\xi(T_{g,bulk}) \sim 0.4$ nm. This value is consistent with estimates for the size of the cooperatively rearranging region (CRR) by Solunov[40] for bulk polyethylene. On the basis of Solunov's estimate of 3.16 CH_2 units in the CRR and a bulk density of 0.75 g/cm^3, we obtain an independent estimate for $\xi(T_{g,bulk}) = \sqrt[3]{V_{CRR}} = 0.46$ nm.

Figure 8a also shows that, for a comparable reduction in length scale, the depression in T_g of the nanofiber geometry is greater than that of the thin film geometry. The disparity in T_g depression is statistically significant, and cannot be attributed to differences in the characteristic length $\xi(T)$. The enhanced T_g depression of the nanofibers may be attributed to differences in the degree of confinement and curvature, as well as to the increase in core energy density with decreasing fiber radius (Figure 4). As the attractive LJ interactions are weaker for fibers with $R_{fiber} < 2.0$ nm, the core internal energy of such small fibers is increased by 10% with respect to a thin film of corresponding half-thickness. This larger core energy density in the case of small nanofibers requires that more energy be withdrawn to reduce inter- and intramolecular motion to the point of vitrification, thus decreasing the glass transition temperature relative to the thin film.

Experiments in free-standing amorphous thin films indicate that the depression of T_g is not a strong function of molecular weight for polymers of low to moderate molecular weight. We also considered the effect of molecular weight on the depression of T_g for PE nanofibers. Figure 10 shows T_g as a function of fiber radius for three different molecular weights, 700 g/mol (C50), 1400 g/mol (C100), and 2100 g/mol (C150). Clearly, we do not observe a significant dependence of the T_g depression on the molecular weight of the polymer for the molecular weights within the simulated range. This observation also justifies application of the layer model to our results, since this model was developed specifically to explain experimental data for thin films in the range of low molecular weights where T_g depression is observed to be molecular weight-independent.

Conclusions

We used MD methods to investigate the size-dependent properties of nanofibers for the prototypical polymer, polyethylene. The diameter of the largest fiber was ~23.0 nm, which is comparable to diameters of nanofibers that can be prepared by electrospinning. In general, our results show that the fibers exhibit bulklike structure and physical properties at the core of the fiber. Near the free surface, significant confinement of the molecules extends approximately one R_g from the GDS toward the fiber core. The interfacial excess energy is 0.022 ± 0.002 J/m^2 and is not dependent on fiber diameter. The T_g of the amorphous PE nanofibers decreases by 50% as R_{fiber} decreases from 2.81 to 0.87 nm, and is not a function of molecular weight over the range considered. Application of a volume averaged layer model for T_g shows that the cooperativity length scale $\xi(T)$ compares well with previous estimates for polyethylene, but cannot explain the greater T_g depression of nanofibers compared to free-standing thin films of comparable thickness. This radius-dependent T_g depression can be attributed at least in part to the increase in the core energy of very small nanofibers ($R_{fiber} < 2.0$ nm). These results show that the physical properties of amorphous polymer nanofibers differ significantly from bulk and their thin film counterparts.

Appendix

If we consider an ellipsoid with semi−major axes of length a, b and c, of which the outermost layer having thickness $\xi(T)$ is considered to be "surface" material with a glass transition temperature $T_g = T_{g,surf}$, and the remaining core material exhibits a glass transition $T_g = T_{g,bulk}$, then a simple volume-averaged T_g can be calculated as

$$T_g = T_{g,bulk} - \left[\frac{(ab+ac+bc)\xi(T_g)}{abc} - \frac{(a+b+c)(\xi(T_g))^2}{abc} + \frac{(\xi(T_g))^3}{abc}\right] \times (T_{g,bulk} - T_{g,surf}) \quad \text{(A1)}$$

For a thin film, $a = h_{1/2}$ and $b = c \to \infty$, resulting in the thin film equation:

$$T_g = T_{g,bulk} - \frac{\xi(T_g)}{h_{1/2}}(T_{g,bulk} - T_{g,surf}) \quad \text{(A2)}$$

For a cylinder, $a = b = R$ and $c \to \infty$, so we obtain the nanofiber result:

$$T_g = T_{g,bulk} - \left[\frac{2\xi(T_g)}{R} - \left(\frac{\xi(T_g)}{R}\right)^2\right](T_{g,bulk} - T_{g,surf}) \qquad \text{(A3)}$$

where the factor of 2 in the linear term is due to the 2-fold symmetry of the cylindrical cross-section.

For a sphere, $a = b = c = R$, so we obtain

$$T_g = T_{g,bulk} - \left[\frac{3\xi(T_g)}{R} - 3\left(\frac{\xi(T_g)}{R}\right)^2 + \left(\frac{\xi(T_g)}{R}\right)^3\right](T_{g,bulk} - T_{g,surf}) \qquad \text{(A4)}$$

where the factor of 3 in the linear and quadratic terms is due to the 3-fold symmetry of the sphere.

Acknowledgment. This work was supported by the Dupont MIT Alliance.

References and Notes

(1) Madden, W. G. *J. Chem. Phys.* **1987**, *87*, 1405−1422.
(2) Mansfield, K. F.; Theodorou, D. N. *Macromolecules* **1990**, *23*, 4430−4445.
(3) Mansfield, K. F.; Theodorou, D. N. *Macromolecules* **1991**, *24*, 6283−6294.
(4) Harris, J. G. *J. Phys. Chem.* **1992**, *96*, 5077−5086.
(5) Kumar, S. K.; Russell, T. P.; Hariharan, A. *Chem. Eng. Sci.* **1994**, *49*, 2899−2906.
(6) Misra, S.; Fleming, P. D.; Mattice, W. L. *J. Comput.-Aided Mater. Design.* **1995**, *2* (2), 101.
(7) He, D. Y.; Reneker, D. H.; Mattice, W. L. *Comput. Theor. Polym. Sci.* **1997**, *7* (1), 19−24.
(8) Rapold, R. F.; Mattice, W. L. *J. Chem. Soc., Faraday Trans.* **1995**, *91*, 2435−2441.
(9) Doruker, P.; Mattice, W. L. *Macromolecules* **1998**, *31*, 1418−1426.
(10) Doruker, P.; Mattice, W. L. *Macromolecules* **1999**, *32*, 194−198.
(11) Doruker, P.; Mattice, W. L. *J. Phys. Chem.* B. **1999**, *103*, 178−183.
(12) Doruker, P. *Polymer* **2002**, *43*, 425.
(13) Vao-soongnern, V.; Doruker, P.; Mattice, W. L. *Macromol. Theory Simul.* **2000**, *9* (1), 1−13.
(14) Vao-Soongnern, V.; Mattice, W. L. *Langmuir*. **2000**, *16*, 6757−6758.
(15) Vao-soongnern, V.; Ozisik, R.; Mattice, W. L. *Macromol. Theory Simul.* **2001**, *10*, 553−563.
(16) Keddie, J. L.; Jones, R. A. L.; Cory, R. A. *Europhys. Lett.* **1994**, *27* (1), 59−64.
(17) Keddie, J. L.; Jones, R. A. L. *Isr. J. Chem.* **1995**, *35* (1), 21−26.
(18) Fukao, K.; Miyamoto, Y. *Phys. Rev. E.* **2000**, *61*, 1743−1754.
(19) Fukao, K.; Miyamoto, Y. *Europhys. Lett.* **1999**, *46*, 649−654.
(20) Tsui, O. K. C.; Russell, T. P.; Hawker, C. J. *Macromolecules* **2001**, *34*, 5535−5539.
(21) Fryer, D. S.; Nealey, P. F.; de Pablo, J. J. *J. Vac. Sci. Technol. B.* **2000**, *18*, 3376−3380.
(22) Ellison, C. J.; Torkelson, J. M. *Nat. Mater.* **2003**, *2* (10), 695−700.
(23) Ellison, C. J.; Torkelson, J. M. *J. Polym. Sci., Part B: Polym. Phys.* **2002**, *40*, 2745−2758.
(24) Keddie, J. L.; Jones, R. A. L.; Cory, R. A. *Faraday Discuss. Chem. Soc.* **1994**, 219−230.
(25) Forrest, J. A.; DalnokiVeress, K.; Stevens, J. R.; Dutcher, J. R. *Phys. Rev. Lett.* **1996**, *77*, 2002−2005.
(26) Forrest, J. A.; DalnokiVeress, K.; Dutcher, J. R. *Phys. Rev. E.* **1997**, *56*, 5705−5716.
(27) Forrest, J. A.; Mattsson, J. *Phys. Rev. E.* **2000**, *61*, R53−R56.
(28) Dalnoki-Veress, E.; Forrest, J. A.; Murray, C.; Gigault, C.; Dutcher, J. R. *Phys. Rev. E.* **2001**, 6303.
(29) Torres, J. A.; Nealey, P. F.; de Pablo, J. J. *Phys. Rev. Lett.* **2000**, *85*, 3221−3224.
(30) Varnik, F.; Binder, K.; Baschnagel, J. *Int. J. Mod. Phys. C.* **2002**, *13*, 799−804.
(31) Varnik, F.; Baschnagel, J.; Binder, K. *Phys. Rev. E.* **2002**, 65.
(32) Varnik, F.; Baschnagel, J.; Binder, K. *J. Non-Cryst. Solids.* **2002**, *307*, 524−531.
(33) Yoshimoto, K.; Jain, T. S.; Nealey, P. F.; de Pablo, J. J. *J. Chem. Phys.* **2005**, 122.
(34) Plimpton, S. *J. Comput. Phys.* **1995**, *117* (1), 1−19.
(35) Paul, W.; Yoon, D. Y.; Smith, G. D. *J. Chem. Phys.* **1995**, *103*, 1702−1709.
(36) Waheed, N.; Lavine, M. S.; Rutledge, G. C. *J. Chem. Phys.* **2002**, *116*, 2301−2309.
(37) Harmandaris, V. A.; Mavrantzas, V. G.; Theodorou, D. N. *Macromolecules.* **1998**, *31*, 7934−7943.
(38) *Polymer Handbook*, 4th ed.; Wiley: New York, 1999.
(39) Capaldi, F. M.; Boyce, M. C.; Rutledge, G. C. *Polymer.* **2004**, *45*, 1391−1399.
(40) Solunov, C. A. *Eur. Polym. J.* **1999**, *35*, 1543−1556.

MA0714666